

# CrystEngComm

Accepted Manuscript



This is an *Accepted Manuscript*, which has been through the Royal Society of Chemistry peer review process and has been accepted for publication.

*Accepted Manuscripts* are published online shortly after acceptance, before technical editing, formatting and proof reading. Using this free service, authors can make their results available to the community, in citable form, before we publish the edited article. We will replace this *Accepted Manuscript* with the edited and formatted *Advance Article* as soon as it is available.

You can find more information about *Accepted Manuscripts* in the [Information for Authors](#).

Please note that technical editing may introduce minor changes to the text and/or graphics, which may alter content. The journal's standard [Terms & Conditions](#) and the [Ethical guidelines](#) still apply. In no event shall the Royal Society of Chemistry be held responsible for any errors or omissions in this *Accepted Manuscript* or any consequences arising from the use of any information it contains.

## ARTICLE

## A cheap and efficient catalyst with ultra high activity for reduction of 4-nitrophenol

Cite this: DOI: 10.1039/x0xx00000x

Weicheng Pan,<sup>a,b,c</sup> Shenghuan Zhang,<sup>a,c</sup> Fei He,<sup>a</sup> Shili Gai,<sup>a</sup> Yanbo Sun,<sup>\*d</sup> and Piaoping Yang<sup>\*a</sup>Received 00th January 2012,  
Accepted 00th January 2012

DOI: 10.1039/x0xx00000x

www.rsc.org/

The ferromagnetic nanoparticles (NPs) prepared by conventional routes usually leads to large particle size for their easy aggregation nature, and the low loading amount greatly limits their application in reduction of 4-nitrophenol (4-NP). In this contribution, well dispersed Ni nanoparticles with small diameter of 7 nm have been supported on mesoporous silica SBA-15 through a facile *in situ* decomposition and reduction strategy. It is found that the as-prepared Ni/SBA-15 can be used as catalyst and exhibits high specific surface area (461 m<sup>2</sup>/g) and ultra high loading amount (574 μg/mg). The well-dispersed and high-loading Ni NPs make the Ni/SBA-15 exhibit excellent catalytic performance in the 4-NP reduction, which is superior to any Ni NPs supported catalysts reported so far and many noble metal supported catalysts. In particular, the magnetic property of Ni/SBA-15 makes it easy to recycle for reuse. This novel synthetic strategy may pave the way for the preparation of other metal nanoparticles supported on different kinds of amorphous silica with high loading capacity and high dispersion.

### 1. Introduction

Use of metal nanoparticles (NPs) as catalyst has gained immense interest due to their unique physical properties, which are significantly different from the bulk materials.<sup>1</sup> Noble metal nanoparticles such as platinum, gold, palladium and silver have already been extensively researched as catalysts.<sup>2-5</sup> Recently, transition metal catalysts, such as nickel, cobalt, copper and iron, are becoming more and more popular than noble metal catalysts because of their markedly lower cost.<sup>6-10</sup> Among them, Ni NPs are the most popular one due to the alternative catalytic and magnetic properties.<sup>11-13</sup> However, smaller particles tend to be easily aggregated due to their large surface area-to-volume ratio.<sup>14</sup> In order to avoid aggregation, the common method is to immobilize the nanoparticles onto solid supports.<sup>15</sup> However, finding a suitable solid support and immobilizing the nanocatalysts on the support with highly dispersion and large loading amounts are of great challenges.

For suitable supports, one would like to have the following two properties: a high specific surface area which can provide large catalytic sites, strong affinity for the catalyst particles so as to immobilize the metal particles with well dispersibility. So far, various solid supports have been used for immobilizing metal nanoparticles such as hollow SiO<sub>2</sub> spheres, polymers, porous carbon, silica nanotubes, carbon nanotubes, graphene oxide, and mesoporous silica.<sup>16-22</sup> Among them, highly ordered mesoporous SBA-15 silica has drawn much attention due to its considerable large surface area of 600-1000 m<sup>2</sup>/g. Furthermore, the uniform pore diameters of 2.0-30.0 nm provide an ideal scaffold for immobilize metal nanoparticles.<sup>23,25</sup> Up to now, various strategies have been developed for the synthesis of mesoporous SBA-15 silica-supported nanostructure materials, which can generally classified into three groups: one is incipient wetness or ion exchange of the metal

precursors into the porous silica support and followed by thermal treatment and reduction with H<sub>2</sub> to form metal nanoparticles.<sup>26</sup> Another is chemical vapor infiltration of the volatile metal precursors and then deposition on the mesoporous silica support.<sup>27</sup> The last one is ultrasonic method to hammer the metal nanoparticles in the silica pores.<sup>28</sup> Although the strategies mentioned above have been extensively applied in the synthesis of SBA-15 silica-supported nanostructure materials, the loading amount and dispersibility of the metal nanoparticles are far from perfection. And the metal nanoparticles generated on the support typically lack of uniformity in size and shape.<sup>29</sup> Furthermore, the low loading amount of metal nanoparticles on SBA-15 greatly limits the application.

As we know, 4-aminophenol (4-AP) is a highly important organic compound which is widely applied in manufacturing analgesic, antipyretic drugs and photographic developer, while 4-nitrophenol (4-NP) is a common organic pollution in industrial and agricultural waste water.<sup>30-32</sup> Therefore, the environmental method is converting 4-NP to 4-AP over metal nanoparticles in the presence of excess NaBH<sub>4</sub>. This method has been a model system to evaluate the catalytic activity of the metal nanoparticles. Various noble metal nanoparticles such as Au, Ag, Pt, Au-Pt and Au-Ag have been extensively used because of their efficient catalytic activities.<sup>33-39</sup> In order to reduce the cost of noble metal catalysts, transition metal particles or composite, such as Ni nanoparticles, Ni/Au nanostructures, reduced graphene oxide/nickel, have become more and more popular.<sup>40-43</sup> However, for the purpose of catching up with the catalytic activities of the noble metal nanoparticles, both tiny, monodisperse nanoparticles and supports with large surface area are necessary.

In this study, we developed a novel method to synthesize Ni/SBA-15 with high loading amount and high dispersion of Ni NPs *via* an *in situ* thermal decomposition and reduction method from silicate

precursor, which is synthesized by hydrothermal reaction. The advantages of this unique synthesized method are facility and the Ni NPs can have ultra small particle size, ultra high loading amount and good dispersion. Furthermore, comparing to other fabrication methods, Ni NPs can bind to the SBA-15 support more firmly. To the best of our knowledge, this is the first time mesoporous SBA-15 has been utilized as precursor (instead of support) for the production of highly dispersed Ni NPs. The Ni/SBA-15 was employed as catalyst to investigate the catalytic performance in reduction of 4-NP, and the stability of the multifunctional catalyst was also studied.

## 2. Experimental Section

### 2.1. Synthesis

**Synthesis of SBA-15.** SBA-15 was synthesized following the literature procedure.<sup>44</sup> The procedure began with dissolving P123 (4.0) in HCl solution (150 mL, 2.0 M) at 40 °C under stirring. TEOS (8.5 g) was added into the reaction container dropwise at 40 °C for 24 h after a homogenous solution formed. Subsequently, the resultant mixture was hydrothermally aged without stirring at 100 °C for 48 h. The products were filtered and washed with distilled water and dried overnight. The organic template was removed by calcination in air at 530 °C for 6 h.

**Synthesis of NiSBA-15.** At room temperature, 0.75 mmol nickel chloride and 10 mmol ammonia chloride were dissolved in 30 mL of deionized water, and then 1 mL ammonia solution (28%) was added under stirring. The color turned to dark green immediately. 40 mg as prepared SBA-15 was added to 10 mL deionized water. Then the above two solution were mixed under ultrasonication and then transferred into a Teflon autoclave (50 mL) and heated of 100 °C for 12 h. After cooling to the room temperature, a green precipitate was collected by centrifugation and washed with deionized water and ethanol three times. NiSBA-15 precursor was finally obtained after dried at 60 °C for 12 h.

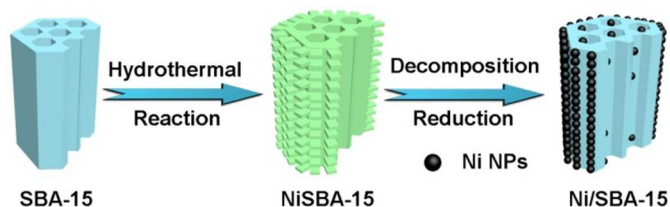
**Synthesis of Ni/SBA-15.** NiSBA-15 silicate precursors were placed in a ceramic boat in the middle of the horizontal tube furnace. And Ni/SBA-15 magnetic catalyst was obtained by heating at 800 °C for 8 h in 5% H<sub>2</sub>/N<sub>2</sub> gas. Black power was collected in the ceramic boat at room temperature.

### 2.2. Catalytic reaction

The aqueous solutions of 4-NP (5 mM) and NaBH<sub>4</sub> (0.2 M) were freshly prepared. 4-NP solution (50 μL), H<sub>2</sub>O (2 mL), and NaBH<sub>4</sub> (1 mL) were added into a quartz cuvette. Then 4 mg as-prepared catalyst or 100 μL catalyst solution (0.1 wt%) was added into the cuvette to started the reaction. Changes in the concentration of 4-NP were monitored by the UV-vis absorption which were recorded in the scanning range of 250–500 nm at room temperature.

### 2.3. Characterization

The crystallographic information of the sample was characterized through X-ray diffraction (XRD, RigakuD/max-TTR-III, Cu K $\alpha$  radiation,  $\lambda = 1.5405 \text{ \AA}$ ). Morphological and compositional investigations were carried out with the field-emission scanning electron microscopy (FESEM, Hitachi S-4800), transmission electron microscopy (TEM) and high-resolution transmission electron microscopy (HRTEM) micrographs which were performed on a FEI Tecnai G<sup>2</sup> S-Twin transmission electron microscope with a field emission gun operating at 200 kV. Images were acquired



**Scheme 1** Schematic illustration for the preparation of Ni/SBA-15.

digitally on a Gatan multiple CCD camera. Specific surface area of tested samples were determined using N<sub>2</sub> adsorption-desorption isotherms at 77K (Micromeritics TriStar 3020 instrument). The specific surface area was calculates by the Brunauer-Emmett-Teller (BET) method, and pore size distribution was calculated from the desorption branch. Magnetization measurements were performed on a MPM5-XL-5 superconducting quantum interference device (SQUID) magnetometer at 300 K. Inductively coupled plasma (ICP) (Thermo iCAP 6000 ICPOES) were used to measure the elemental compositions for the above studied samples. The absorbance of 4-NP was obtained on a UV-vis spectrophotometer (TU-1901).

## 3. Results and discussion

### 3.1. Characterization of Ni/SBA-15

Scheme 1 depicts the synthetic strategy of well dispersed Ni NPs on SBA-15. The SBA-15 template was first synthesized through a classical method using P123 as the template and TEOS as the precursor. Then, the lamellar structured nickel silicate (NiSBA-15) was obtained by hydrothermal reaction in the alkaline condition at high temperature. This hydrothermal reaction involved the process of breaking silica chains of mesoporous SBA-15 to form silicate-ion groups and then reacting with nickel ions to form nickel silicate in the solution. Finally, monodisperse Ni NPs supported on SBA-15 were obtained through an *in situ* decomposition and reduction procedure in the hydrogen atmosphere at high temperature.

Fig. 1 shows the XRD patterns of the as-prepared precursor and final product, respectively. The XRD diffractions of the as-prepared precursor can be indexed to nickel silicate hydrates. The sharp diffractions of Ni/SBA-15 can be well indexed to cubic-phased Ni (JCPDS No. 04-0805). The low broad band at  $2\theta = 22^\circ$  is assigned to amorphous silica. The XRD result indicates that nickel silicate precursor has been completely converted to metal and amorphous silica. The broad peaks indicate the nanosized nature of Ni NPs. The average crystallite size of Ni NPs calculated from the Scherrer equation is 7.2 nm, agreeing well with the following TEM result.

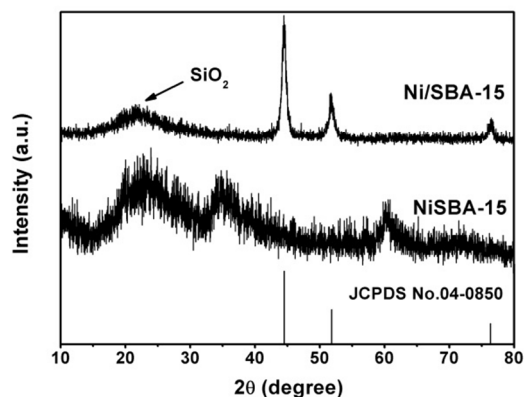


**Fig. 1** Wide-angle XRD patterns of NiSBA-15, Ni/SBA-15 and standard data of the cubic Ni..

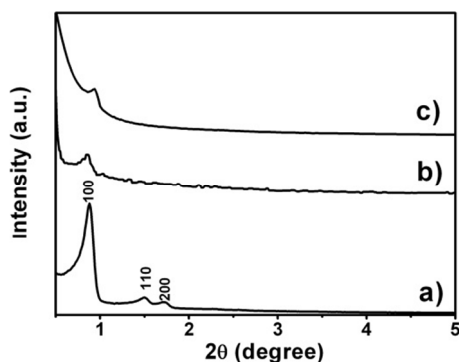


Fig. 2 Low-angle XRD patterns of the a) SBA-15, b) NiSBA-15 and c) Ni/SBA-15.

Fig. 2 shows the respective low-angle XRD patterns of SBA-15 template, nickel silicate and Ni/SBA-15. In the low-angle XRD pattern of SBA-15 template (Fig. 2a), the three characteristic peaks can be indexed as (100), (110), and (200) of the two-dimensional  $p6mm$  hexagonal mesostructure.<sup>45</sup> It is found that only the characteristic peak of (100) is preserved for NiSBA-15 (Fig. 2b) and Ni/SBA-15 (Fig. 2c), which indicates the hexagonal mesostructure still exists. However, the intensity of NiSBA-15 and Ni/SBA-15 is much lower than that of SBA-15, revealing the order of mesoporous structure is decreased.

The low-magnification SEM images of SBA-15, NiSBA-15 and Ni/SBA-15 are displayed in Fig. S1. It is found that all of the samples present rod-like structure with the length about 30  $\mu\text{m}$ . From the high-magnification SEM images (Fig. S1d-f), we can see numerous nanoparticles, a large number of micropores and petal-like structure on the surface of Ni/SBA-15. Fig. 3 gives the TEM images of SBA-15 and NiSBA-15. The low-magnification TEM images (Fig. 3a) exhibit the rod like structure of SBA-15. From Fig. 3b, it is clear that the center-to-center distances of adjacent channels are 10.0 nm. After hydrothermal reaction, the rod-like structure can still be seen for NiSBA-15 (Fig. 3c). However, the surface of NiSBA-15 becomes much rougher. In Fig. 3d, numerous uniform petal-like nanosheets with the length of about 100 nm are found. The channels cannot be distinguished due to the covered petal-like nanosheets. The petal-like structure is generated *via* the *in situ* reaction process, after the nickel ions react with the silicate ions on the surface, the inner silica chains will dissolve and move to the surface and go on reaction.<sup>46</sup> Therefore, the channels on the surface will take part in the reaction and disappear, which make the channels less ordered.

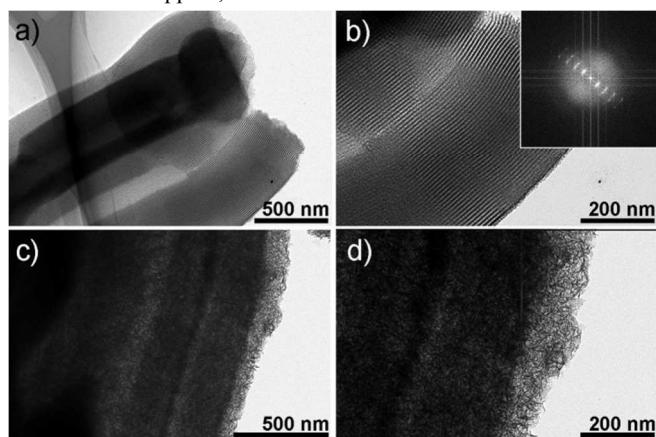


Fig. 3 a) Low-, b) high-magnification TEM images of SBA-15, c) low-, d) high-magnification TEM image of NiSBA-15.

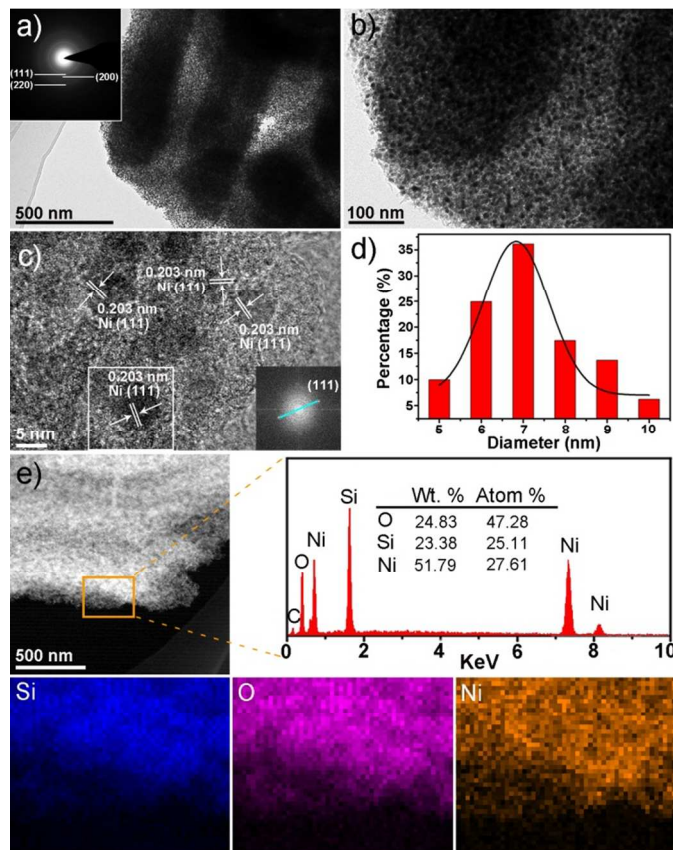
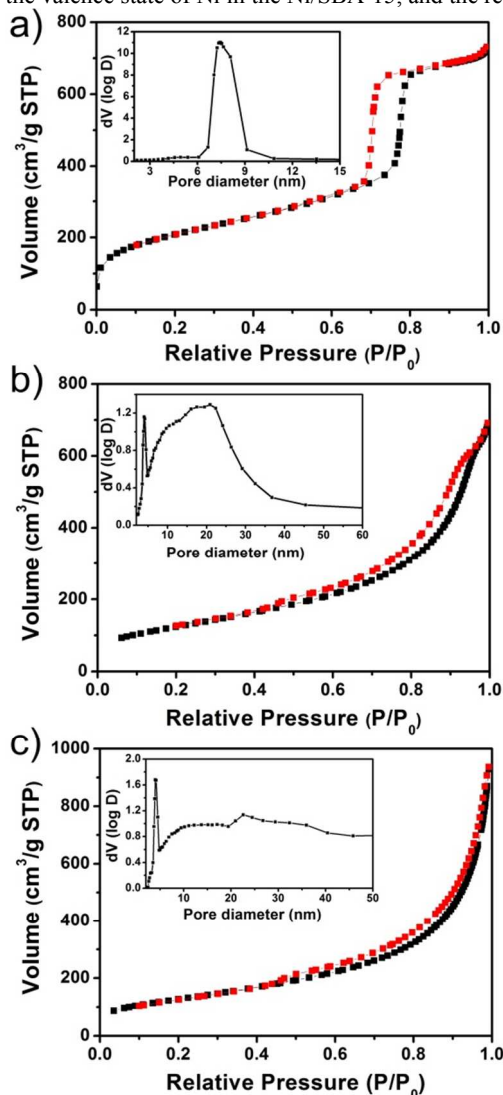


Fig. 4 a) Low-, b) high-magnification TEM images (inset (a) is the SAED pattern), c) HRTEM image (inset is corresponding FFT pattern), d) size distribution histogram of the Ni NPs, and e) EDS and mapping of Ni/SBA-15.

From the TEM images of Ni/SBA-15 (Fig. 4), we can see that the rod-like SBA-15 is surrounded by numerous tiny particles instead of thin nanosheets. However, the channels are faintly visible, which may be due to the high loading amount of Ni NPs. The inset of Fig. 4a is the selected area electron diffraction (SAED) pattern of Ni/SBA-15. The presence of the concentric rings further confirms the formation of the cubic-phase Ni, which corresponds to above XRD result. Fig. 4c displays the HRTEM image of Ni/SBA-15, it is clear that all of the Ni NPs are near-perfect spheres with the diameter of about 7 nm. The lattice fringes can be easily seen and the distance of the adjacent lattice fringes (marked by the arrows) is determined to be about 0.20 nm which correspond well to the  $d_{111}$  spacing of cubic-Ni (JCPDS No. 04-0850). A pair of diffraction spots is displayed (inset in Fig. 4c), which reveals the crystalline nature of the Ni and can be calculated to the (111) planes of cubic Ni. Fig. 4d shows the size distribution histogram of the Ni NPs calculated from the magnified TEM image of Ni/SBA-15 (Fig. 4b) and the black line is a curve fitting with a Gaussian function. Ni NPs are uniform in the diameter with a relatively narrow distribution, and the average size calculated from the curve is 6.9 nm. In the EDS (Fig. 4e), only Si, O, Ni elements can be found except for C from the carbon conductive tape. The respective mass percentage and atom weight percent of Ni is 52.79 and 27.61, which reveals the high Ni loading amounts has been achieved. The result is basically in accordance with the ICP result (57.4 wt.%). Additionally, from the TEM mapping of Ni/SBA-15 (Fig. 4e), we can see that Ni atoms are uniformly dispersed on the surface of SBA-15 with high loading amount. This can be attributed to the unique *in situ* thermal decomposition and subsequent

reduction process. To certify the new material, we used XPS to confirm the valence state of Ni in the Ni/SBA-15, and the result is



**Fig. 5**  $N_2$  adsorption-desorption isotherms of a) SBA-15, b) NiSBA-15, c) Ni/SBA-15 and their corresponding pore size distributions (insets).

shown in Fig. S3. In the XPS spectra, the peaks located at 856.2 and 862.3 eV are assigned to the binding energy of Ni  $2p_{3/2}$  and Ni  $2p_{1/2}$ , which reveals that zero value Ni is obtained after reduction.<sup>49,50</sup>

$N_2$  adsorption-desorption isotherm and the corresponding pore size distribution (inset) of SBA-15, NiSBA-15 and Ni/SBA-15 are displayed in Fig. 5. Each isotherm can be classified to a type-IV isotherm with a hysteresis loop, indicating the presence of textural mesopores. Table 1 summarizes the textural parameters of SBA-15, NiSBA-15 and Ni/SBA-15. The BET surface areas of NiSBA-15 and Ni/SBA-15 are 449  $m^2/g$  and 461  $m^2/g$ , and the average pore sizes are 10.0 nm and 13.3 nm, respectively. Both of them show large BET surface areas indicating reduction have little effect on BET surface area. However, comparing to SBA-15 template, the average pore sizes of NiSBA-15 and Ni/SBA-15 are larger. This can be attributed to the collapse of some ordered channel. Furthermore, some Ni NPs generated after calcination may block ordered channel or stack to form secondary mesopores, which lead to the decrease of pore size. Above all, the large BET surface areas and remained ordered channel of Ni/SBA-15 suggest the promising application in catalytic reaction.

Fig. 6 shows the magnetization curve of Ni/SBA-15 at room temperature. The saturation magnetization value is 0.26 emu/g and **Table 1** The BET surface area, total pore volume, and average pore size of SBA-15, NiSBA-15, and Ni/SBA-15.

	BET surface area ( $m^2/g$ )	Pore volume ( $cm^3/g$ )	Average pore size (nm)
SBA-15	727	1.1	7.3
NiSBA-15	449	1.1	10.0
Ni/SBA-15	461	1.5	13.3

nearly no coercivity or remanence can be found. It is well known that magnetic NPs smaller than 20 nm are usually superparamagnetic at room temperature because of the higher thermal fluctuation energy compared with energy.<sup>47,48</sup> And the enlarged magnetization curve (inset in Fig. 6) reveals that the coercivity is 32 Oe, which is very close to the superparamagnetic state. The photograph of the magnetic separation (inset in Fig. 6) demonstrates the catalyst can be easily manipulated by an external magnetic field, which makes it possible to be recycled for reuse.

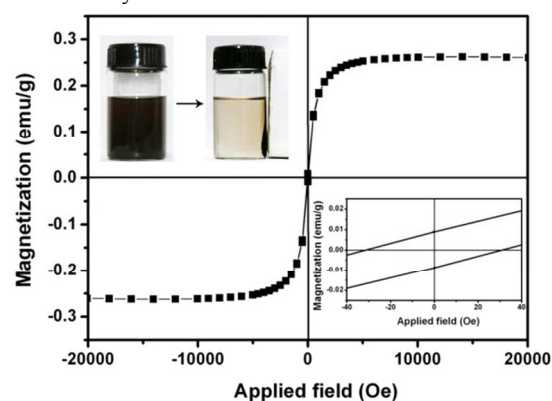


**Fig. 6** Magnetization curve of Ni/SBA-15 at room temperature. The inset is the photograph for the magnetic separation (up left) and the enlargement near origin (low right).

### 3.2. Catalytic performance of Ni/SBA-15 catalyst

It is well known that that the catalytic reduction of 4-NP with an excess amount of  $NaBH_4$  is fast in presence of metallic surfaces,<sup>51-53</sup> and the catalytic performance of Ni/SBA-15 is evaluated by this reaction in this work. In Fig. 7a, the UV-vis absorbance band centered at 317 nm, 400 nm and 295 nm is assigned to 4-NP, 4-nitrophenolate ion generated after adding  $NaBH_4$  and 4-AP, respectively. The corresponding color is light yellow, bright yellow and finally colorless after the completely reaction (inset in Fig. 7a). Fig. 7b reveals that the reaction cannot be performed without catalyst. When we used the amount of 4 mg catalyst, the reaction was completed in 40 s, which is so quick that the process cannot be effectively monitored (Fig. S2). Hence, we reduced the catalyst to 0.1 mg (0.1 wt.%) for catalyzing the reduction of 4-NP. Fig. 7c presents the UV-vis spectra of the 4-NP monitored at different time during the process of the whole reaction. The complete reaction time is 18 min. And along with the decrease of the absorbance band at 400 nm, a new peak at 295 nm formed indicating the formation of 4-AP. The catalytic mechanism for 4-NP reduction relies on the electrons from the  $BH_4^-$  donor to the acceptor 4-NP. Electron transfer (ET) to the metal NPs at first, and then the hydrogen atom was formed from the hydride, attacking 4-NP molecules to reduce it. This ET induced hydrogenation of 4-NP occurs spontaneously. It is also reported that metal NPs play a role in storing electron after ET from the hydride.<sup>54</sup> And the reduction rate can be assumed to be independent of  $NaBH_4$  because the initial concentration of the

NaBH<sub>4</sub> solution is very high, which can be considered as a constant throughout the whole reduction process. The kinetic equation can be

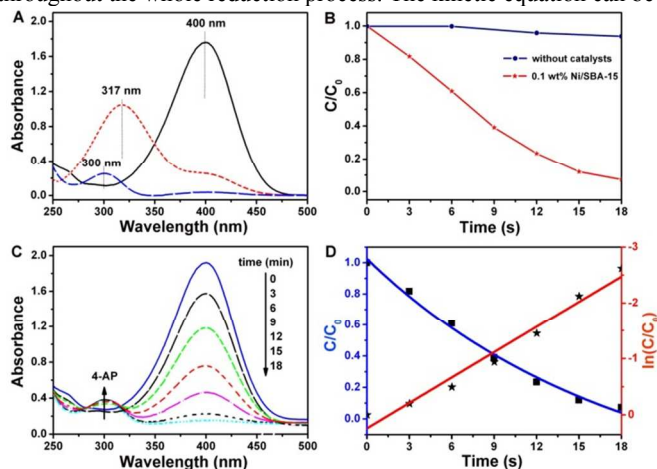


**Fig. 7** a) UV-vis absorption spectra of 4-NP, 4-nitrophenolate, and 4-AP; b)  $C/C_0$  versus reaction time for the reduction of 4-NP at the peak position of 4-NP (400 nm) using bare solution (black line) and 0.1 wt.% Ni/SBA-15 (red line) as catalysts; c) UV-vis spectra of the catalytic reduction of 4-NP to 4-AP developed at different reaction times; d)  $C/C_0$  and  $\ln(C/C_0)$  versus time for the reduction of 4-NP over 0.1 wt.% Ni/SBA-15. The ratio of 4-NP concentration ( $C_t$  at time  $t$ ) to its initial value  $C_0$  is directly represented by the relative intensity of the respective absorption peak at 400 nm.

written as  $-dC/dt = dA/dt = kCt = kAt$  or  $\ln(C/C_0) = \ln(A/A_0) = -kt$ , where  $C$  is the concentration of 4-NP at time  $t$  and  $k$  is the apparent rate constant.<sup>55</sup> Therefore, this pseudo first-order kinetic equation can be applied to evaluate the catalytic rate. The  $\ln(C/C_0)$  versus reaction time plot displayed in Fig. 7d (red line) exhibits a good linear correlation with reaction time and the rate constant  $k$  is calculated to be  $0.003 \text{ s}^{-1}$ . However, it is not entirely appropriate to compare different catalysts because the catalyst concentration directly affects the rate constant. Therefore, the parameter  $\kappa$  which is the ratio of the rate constant  $k$  to the total amounts of the catalysts was introduced to evaluate the catalytic performance of different catalysts. Table S1 gives the comparison of catalytic activities in our work and previously reported. It can be found that the as-prepared Ni/SBA-15 catalyst exhibits highest catalytic activity ( $\kappa = 30 \text{ s}^{-1} \text{ g}^{-1}$ ). As far as we know, the catalytic activity of our Ni/SBA-15 for 4-nitrophenol reduction is obviously higher than any Ni supported catalysts reported.<sup>42,56–58</sup> It should be noted that it is also higher than many noble metal supported catalysts.<sup>32,35,59–61</sup>

The super high catalytic rate can be due to the following three factors: one is tiny Ni NPs which provide more active center for reduction. Another is SBA-15 support with large surface area which can load large amount of Ni NPs thus providing larger reaction areas.

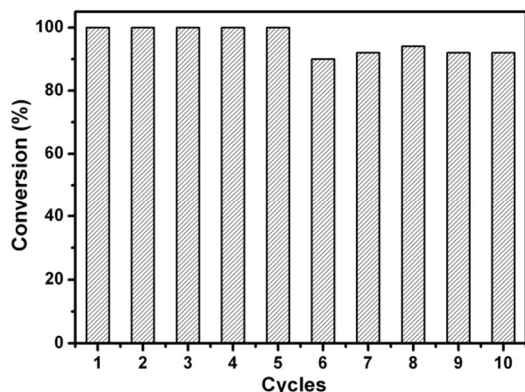


**Fig. 8** The conversion versus cycles of Ni/SBA-15 as a catalyst for the reduction of 4-NP with NaBH<sub>4</sub>.

And last, well monodisperse of Ni NPs provide larger surface area for reduction. Besides the super high catalytic rate, another advantage of Ni/SBA-15 is the stability and reusability. The magnetic properties make it easy for separation from the solution. Fig. 8 shows the reusability of Ni/SBA-15 catalysts for the reduction of 4-NP. The results demonstrate that the catalyst still remain high catalytic activity even after ten reaction cycles. This can be attributed to the high dispersion, tiny particle size and especially firm attachment of Ni NPs to the support deriving from the unique *in-situ* decomposition and reduction route. The respective Ni content before and after recycling 5 times is  $574 \mu\text{g}/\text{mg}$  and  $539 \mu\text{g}/\text{mg}$ , and the values before and after recycling 10 times is  $574 \mu\text{g}/\text{mg}$  and  $397 \mu\text{g}/\text{mg}$  determined by the ICP analysis. This result indicates that there is relatively low leaching of Ni NPs with the repeated magnetic separation.

## Conclusions

In summary, we have synthesized Ni/SBA-15 catalysts with high surface area and super catalytic activity by a novel and rational strategy which is *in situ* decomposition and reduction of inorganic salt precursor. Ni NPs (about 7 nm) was monodisperse on mesoporous SBA-15 with high loading amounts. The sample exhibits excellent catalytic performance in the 4-NP reduction. The catalytic activity is higher than any other supported Ni NPs and many supported noble metal catalysts. The as prepared Ni/SBA-15 catalyst exhibits several advantages: high catalytic performance, easy for reuse and low cost. In particular, the significance of this new synthesis method is expected as a general technique for synthesis of other metal nanoparticles supported on different kinds of amorphous silica with large loading capacity and well dispersion, which should be promising efficient catalysts.

## Acknowledgements

This work was supported by financial supports from National Natural Science Foundation of China (NSFC 21271053, 21401032, 51472058), Natural Science Foundation of Heilongjiang Province (B201403), Harbin Sci.-Tech. Innovation Foundation (2014RFQXJ019), Program for Science & Technology Innovation Talents in Universities of Henan Province (2012HASTIT037), and Science and Technology Research Key Project of Education Department Henan Province (12A530003, 14A530003).

## Notes and references

- Key Laboratory of Superlight Materials and Surface Technology, Ministry of Education, College of Material Science and Chemical Engineering, Harbin Engineering University, Harbin 150001, P. R. China. E-mail: [yangpiaoping@hrbeu.edu.cn](mailto:yangpiaoping@hrbeu.edu.cn)
- College of Chemical Engineering and Food Engineering, Zhongzhou University, Zhengzhou 450044, P. R. China
- The authors contributed equally.
- State Key Laboratory of Theoretical and Computational Chemistry, Jilin University, Changchun 130023, P. R. China  
E-mail: [syb@jlu.edu.cn](mailto:syb@jlu.edu.cn)

† Electronic Supplementary Information (ESI) available: SEM images of SBA-15, NiSBA-15 and Ni/SBA-15; UV-vis spectra of successive reduction of 4-NP using 4 mg Ni/SBA-15 as catalyst; comparison of the activity parameter  $\kappa$  of composite Ni catalysts and noble catalysts for the reduction of 4-nitrophenol; XPS spectrum of Ni/SBA-15 Sample. See DOI: 10.1039/b000000x

- 1 S. Shylesh, V. Schuenemann and W. R. Thiel, *Angew. Chem. Int. Ed.*, 2010, **49**, 3428.
- 2 Y. Sun and C. Lei, *Angew. Chem. Int. Ed.*, 2009, **48**, 6824.
- 3 H. Lee, S. E. Habas, S. Kweskin, D. Butcher, G. A. Somorjai and P. Yang, *Angew. Chem. Int. Ed.*, 2006, **45**, 7824.
- 4 M. D. Hughes, Y.-J. Xu, P. Jenkins, P. McMorn, P. Landon, D. I. Enache, A. F. Carley, G. A. Attard, G. J. Hutchings and F. King, *Nature*, 2005, **437**, 1132.
- 5 S. Pande, S. K. Ghosh, S. Praharaaj, S. Panigrahi, S. Basu, S. Jana, A. Pal, T. Tsukuda and T. Pal, *J. Phys. Chem. C*, 2007, **111**, 10806
- 6 Z. Wang, and R. T. Yang, *J. Phys. Chem. C*, 2010, **114**, 5956.
- 7 X. W. Xie, Y. Li, Z. Q. Liu, M. Haruta and W. J. Shen, *Nature*, 2009, **458**, 746.
- 8 S. Bhaviripudi, X. T. Jia, M. S. Dresselhaus and J. Kong, *Nano Lett.*, 2010, **10**, 4128.
- 9 W. Chen, Z. Fan, X. Pan and X. Bao, *J. Am. Chem. Soc.*, 2008, **130**, 9414.
- 10 H. M. Torres Galvis, J. H. Bitter, C. B. Khare, M. Ruitenbeek, A. I. Dugulan and K. P. de Jong, *Science*, 2012, **335**, 835
- 11 Ö. Metin, V. Mazumder, S. Özkaz and S. Sun, *J. Am. Chem. Soc.*, 2010, **132**, 1468.
- 12 H.-S. Kim, H. Lee, K.-S. Han, J.-H. Kim, M.-S. Song, M.-S. Park, J.-Y. Lee and J.-K. Kang, *J. Phys. Chem. B*, 2005, **109**, 8983.
- 13 L. Wang and R. T. Yang, *J. Phys. Chem. C*, 2008, **112**, 12486.
- 14 A. S. K. Hashmi and G. J. Hutchings, *Angew. Chem. Int. Ed.*, 2006, **45**, 7896.
- 15 X. Chen, H. Y. Zhu, J. C. Zhao, Z. T. Zheng and X. P. Gao, *Angew. Chem. Int. Ed.*, 2008, **47**, 5353.
- 16 K. Nielsch, F. J. Castano, S. Matthias, W. Lee and C. A. Ross, *Adv. Eng. Mater.*, 2005, **7**, 217.
- 17 X. Pan and X. Bao, *Chem. Commun.*, 2008, **47**, 6271
- 18 R. Lv, T. Cui, M. S. Jun, Q. Zhang, A. Cao, D. S. Su, Z. Zhang, S. H. Yoon, J. Miyawaki, I. Mochida and F. Kang, *Adv. Funct. Mater.*, 2011, **21**, 999.
- 19 J. Lee, J. C. Park and H. Song, *Adv. Mater.*, 2008, **20**, 1523.
- 20 J. Guo and K. S. Suslick, *Chem. Commun.*, 2012, **48**, 11094.
- 21 Z. Zhang, C. Shao, P. Zou, P. Zhang, M. Zhang, J. Mu, Z. Guo, X. Li, C. Wang and Y. Liu, *Chem. Commun.*, 2011, **47**, 3906.
- 22 R. Zhao, D. Ji, G. Lv, G. Qian, L. Yan, X. Wang and J. Suo, *Chem. Commun.*, 2004, 904.
- 23 Z.-J. Wang, Y. Xie and C.-J. Liu, *J. Mater. Chem.*, 2008, **112**, 19818.
- 24 A. Janssen, C.-M. Yang, Y. Wang, F. Schüth, A. Koster and K. De Jong, *J. Phys. Chem. B*, 2003, **107**, 10552.
- 25 H. Song, R. M. Rioux, J. D. Hoefelmeyer, R. Komor, K. Niesz, M. Grass, P. Yang and G. A. Somorjai, *J. Am. Chem. Soc.*, 2006, **128**, 3027.
- 26 C.-M. Yang, P.-H. Liu, Y.-F. Ho, C.-Y. Chiu and K.-J. Chao, *Chem. Mater.*, 2003, **15**, 275.
- 27 J. R. A. Sietsma, J. D. Meeldijk, J. P. den Breejen, M. Versluijs-Helder, A. J. van Dillen, P. E. de Jongh and K. P. de Jong, *Angew. Chem. Int. Ed.*, 2007, **46**, 4547.
- 28 H. Li, R. Wang, Q. Hong, L. Chen, Z. Zhong, Y. Koltypin, J. Calderon-Moreno and A. Gedanken, *Langmuir*, 2004, **20**, 8352.
- 29 H. Song, R. M. Rioux, J. D. Hoefelmeyer, R. Komor, K. Niesz, M. Grass, P. D. Yang and G. A. Somorjai, *J. Am. Chem. Soc.*, 2006, **128**, 3027.
- 30 C. V. Rode, M. J. Vaidya and R. V. Chaudhari, *Org. Process. Res. Dev.*, 1999, **3**, 465.
- 31 S. Saha, A. Pal, S. Kundu, S. Basu and T. Pal, *Langmuir*, 2009, **26**, 2885.
- 32 Y. H. Deng, Y. Cai, Z. Sun, J. Liu, C. Liu, J. Wei, W. Li, C. Liu, Y. Wang and D. Zhao, *J. Am. Chem. Soc.*, 2010, **132**, 8466.
- 33 K. Jiang, H.-X. Zhang, Y.-Y. Yang, R. Mothes, H. Lang and W.-B. Cai, *Chem. Commun.*, 2011, **47**, 11924.
- 34 F.-H. Lin and R.-A. Doong, *J. Mater. Chem. C*, 2011, **115**, 6591-6598.
- 35 Y. Lu, J. Yuan, F. Polzer, M. Drechsler and J. Preussners, *ACS Nano*, 2010, **4**, 7078.
- 36 L. Zhou, C. Gao and W. Xu, *Langmuir*, 2010, **26**, 11217.
- 37 J. Han, P. Fang, W. Jiang, L. Li and R. Guo, *Langmuir*, 2012, **28**, 4768.
- 38 M. H. Rashid and T. K. Mandal, *Adv. Funct. Mater.*, 2008, **18**, 2261.
- 39 X. Zhang and Z. Su, *Adv. Mater.*, 2012, **24**, 4574.
- 40 Z. Ji, X. Shen, G. Zhu, H. Zhou and A. Yuan, *J. Mater. Chem.*, 2012, **22**, 3471.
- 41 S. Sarkar, A. K. Sinha, M. Pradhan, M. Basu, Y. Negishi and T. Pal, *J. Phys. Chem. C*, 2010, **115**, 1659.
- 42 Z. Jiang, J. Xie, D. Jiang, J. Jing and H. Qin, *CrystEngComm*, 2012, **14**, 4601.
- 43 S. H. Zhang, S. L. Gai, S. J. Ding, L. Lei and P. P. Yang, *Nanoscale*, 2014, **6**, 11181.
- 44 D. Zhao, J. Feng, Q. Huo, N. Melosh, G. H. Fredrickson, B. F. Chmelka and G. D. Stucky, *Science*, 1998, **279**, 548.
- 45 D. Zhao, Q. Huo, J. Feng, B. F. Chmelka and G. D. Stucky, *J. Am. Chem. Soc.*, 1998, **120**, 6024.
- 46 Y. Q. Wang, G. Z. Wang, H. Q. Wang, C. H. Liang, W. P. Cai and L. D. Zhang, *Chem.-Eur. J.*, 2010, **16**, 3497.
- 47 Y. Lee, J. Lee, C. J. Bae, J. G. Park, H. J. Noh, J. H. Park and T. Hyeon, *Adv. Funct. Mater.*, 2005, **15**, 503.
- 48 D. Chen, J. Li, C. Shi, X. Du, N. Zhao, J. Sheng and S. Liu, *Chem. Mat.*, 2007, **19**, 3399.
- 49 B. J. Li, H. Q. Cao, J. F. Yin, Y. A. Wu and J. H. Warner, *J. Mater. Chem.*, 2012, **22**, 1876.
- 50 T. T. Chen, F. Deng, J. Zhu, C. F. Chen, G. B. Sun, S. L. Ma and X. J. Yang, *J. Mater. Chem.*, 2012, **22**, 15190.
- 51 T. K. Sau, A. Pal and T. Pal, *J. Phys. Chem. B*, 2001, **105**, 9266.
- 52 K. Hayakawa, T. Yoshimura and K. Esumi, *Langmuir*, 2003, **19**, 5517.
- 53 Y. Lu, Y. Mei, M. Ballauff and M. Drechsler, *J. Phys. Chem. B*, 2006, **110**, 3930.
- 54 J.-P. Deng, W.-C. Shih and C.-Y. Mou, *J. Phys. Chem. C*, 2007, **111**, 9723.
- 55 M. Schrinner, M. Ballauff, Y. Talmon, Y. Kauffmann, J. Thun, M. Möller and J. Breu, *Science*, 2009, **323**, 617.
- 56 N. Sahiner, H. Ozay, O. Ozay and N. Aktas, *Appl. Catal. A-gen.*, 2010, **385**, 201.
- 57 Z. Jiang, J. Xie, D. Jiang, X. Wei and M. Chen, *CrystEngComm*, 2013, **15**, 560.
- 58 S. Senapati, S. K. Srivastava, S. B. Singh and H. N. Mishra, *J. Mater. Chem.*, 2012, **22**, 6899.
- 59 B. Guan, X. Wang, Y. Xiao, Y. Liu and Q. Huo, *Nanoscale*, 2013, **5**, 2469.
- 60 J. Zheng, Y. Dong, W. Wang, Y. Ma, J. Hu, X. Chen and X. Chen, *Nanoscale*, 2013, **5**, 4894.
- 61 S. Tang, S. Vongehr and X. Meng, *J. Mater. Chem.*, 2010, **20**, 5436.

Ni/SBA-15 catalyst with ultra small particle size (7 nm), good dispersion, and ultra high loading amount (57.4%) of Ni nanoparticles was prepared by a unique *in situ* thermal decomposition and reduction route. The magnetic Ni/SBA-15 catalyst exhibits excellent catalytic activity and stability for 4-nitrophenol reduction.

